Fermi surface of iron under pressure

W. B. Johnson* and J. R. Anderson
Department of Physics and Astronomy, University of Maryland, College Park, Maryland 20742

D. A. Papaconstantopoulos
Naval Research Laboratory, Washington, D.C. 20375
(Received 26 October 1983)

The augmented-plane-wave (APW) method was used to calculate spin-polarized energy bands for body-centered-cubic iron at the normal lattice constant and at lattice spacings corresponding to approximate pressures of 128 and 256 kbar. Both nonrelativistic and semirelativistic energy bands at each pressure were determined with the use of potentials that incorporated the von Barth—Hedin formalism for exchange and correlation. The APW method was used to generate the energy bands at 55 $\vec{k}$ points of an irreducible wedge in the Brillouin zone; then a Slater-Koster Hamiltonian, fitted to the APW results, was used to generate the energy bands at 1785 $\vec{k}$ points in the irreducible wedge and to calculate extremal areas of the Fermi surface and their pressure derivatives. To improve agreement with experiment, the first-principles spin-polarized energy bands were rigidly shifted for each lattice spacing by an amount necessary to reproduce the experimental magneton number. The orders of magnitude of the calculated pressure derivatives of the extremal areas were 10^{-4}/kbar for the spin-up electron *s-d* piece, -10^{-4}/kbar for the spin-down hole octahedron at symmetry point H, 10^{-3}/kbar for the spin-up hole pockets at point H and the electron octahedron at point Γ, and 10^{-2}/kbar for the spin-down electron ball.

I. INTRODUCTION

The first augmented-plane-wave (APW) calculation for iron was done by Wood in 1962.[1] His calculation was neither self-consistent nor spin polarized. More recently, Callaway and Wang[2] performed a self-consistent, spin-polarized calculation for iron using a linear combination of Gaussian orbitals (LCGO) method. Although they considered several different forms for the exchange, they found the best agreement with experimental data for the exchange and correlation potential of von Barth and Hedin.[3] Moruzzi *et al.*[4] performed a Kohn-Korringa-Rostoker (KKR) calculation on iron also using the von Barth—Hedin potential, but they did not calculate the Fermi surface. Vinokurova *et al.*,[5] using a model KKR Hamiltonian, examined the influence of pressure on the electronic structure of iron.

A principal experimental method for studying the Fermi surface of iron has been the de Haas—van Alphen (dHvA) effect.[6,7] Recently, Lonzarich[8] remeasured dHvA oscillations for some small pieces of the Fermi surface and also reinterpreted some of Baraff's data.[7] Data from Shubnikov—de Haas oscillations[9] in the transverse magnetoresistance supported Lonzarich's reinterpretation.

There have been only two experimental studies of the influence of pressure on the Fermi surface of iron and they have been measurements of the dHvA effect for a single piece of the Fermi surface.[8,10] We have examined the pressure dependence of the Fermi surface of iron by calculating the energy bands and the corresponding Fermi surface at three lattice spacings in order to provide a model for future experimental studies. Because there is a phase transition in iron from the bcc to the hcp structure at a pressure of 130 kbar,[11] our highest-pressure calculation, corresponding to 256 kbar, does not represent a ground state of iron. The purpose of the calculation at 256 kbar was to check for a linear variation of the extremal areas of the Fermi surface with pressure.

Using the von Barth—Hedin exchange and correlation potential, we calculated first-principles energy bands that were both spin polarized and self-consistent. We determined both nonrelativistic and semirelativistic (i.e., spin-orbit interaction neglected) energy bands at three lattice spacings: at the lattice spacing at atmospheric pressure (5.4057 a.u.), at a lattice spacing 2.5% smaller (128 kbar), and at another 5% smaller (256 kbar). The correspondence between lattice constant and pressure was found by using the room-temperature value of the compressibility[12] (5.84×10^{-4}/kbar).

Our calculated Fermi surface corresponding to the nonrelativistic, first-principles energy bands at the normal lattice constant did not agree with the experimental Fermi surface as closely as the Fermi surface calculated by Callaway and Wang. Moreover, the topology of the Fermi surface found from our semirelativistic calculation did not agree with the topology of the experimental Fermi surface. The magneton number for the nonrelativistic calculation at the normal lattice constant was 5% larger than the experimental magneton number (2.12),[13] while the magneton number for the semirelativistic calculation was 15% larger. Even though the error in the magneton number appeared to be small, it translated into a larger error in the Fermi surface. Therefore, for the purpose of predicting the variation of the Fermi surface under hydrostatic

pressure we corrected our first-principles energy bands by rigidly shifting them until both the experimental magneton number and the total number of valence electrons were obtained. The Fermi surfaces so obtained agreed much better with the experimental data.

II. METHOD OF COMPUTATION

Both nonrelativistic (NR) and semirelativistic (SR) APW calculations were performed using the same numerical methods[14] used in a previous calculation on spin-polarized nickel.[15] In the SR calculation a relativistic APW was defined at each point in $\vec{k}$ space by solving the Dirac equation inside a muffin-tin sphere and matching the solution to a plane wave in the interstitial region between the muffin-tin spheres. Solving the Dirac equation led to a differential equation[16] that explicitly exhibited a mass-velocity term, a Darwin term, and a spin-orbit term, which would require the energy bands to change as the orientation of the magnetic field changed.[17] Since inclusion of the spin-orbit term would require the recalculation of self-consistent energy bands for different directions of the magnetic field, this term was dropped. When the spin-orbit term is omitted, the semirelativistic formalism is obtained, and when the speed of light in the Dirac equation is made infinite, the nonrelativistic formalism is obtained.

Atomic charge densities were generated with the $(3d)^8(4s)^0$ atomic configuration for the spin-up charge density, and the $(3d)^6(4s)^2$ atomic configuration for the spin-down charge density. These atomic configurations were chosen for two reasons. First, they gave a magneton number of 2.0 for the first iteration, and this was close to the experimental magneton number. It was important to start close to the experimental magneton number because, if the starting magneton number were too far away, it would not converge to a value close to the experimental magneton number after subsequent iterations.[18,19] Second, the discontinuity in the muffin-tin potential at the edge of the muffin-tin sphere was minimized at about 100 mRy by using these starting configurations.

The atomic charge densities were used to generate the starting crystal potential in the muffin-tin form. In this step, the von Barth—Hedin exchange and correlation potential was added to the ordinary Coulomb potential found by solving Poisson's equation, and thus the muffin-tin potential for the spin-up electrons was different from the muffin-tin potential for the spin-down electrons. In calculating the potential, the muffin-tin spheres were chosen just large enough to touch.

The muffin-tin potential was used to calculate $1s$, $2s$, and $2p$ atomic energy levels and charge densities. Because these inner levels were well localized within the muffin-tin sphere, they were treated as atomiclike. For the NR calculations, the program of Herman and Skillman[20] was used to calculate the inner levels and corresponding charge densities, while the program of Liberman *et al.*[21] was used for the SR calculation. In both cases, the $1s$, $2s$, and $2p$ electrons formed a soft core that was allowed to change at each iteration as the muffin-tin potential changed.

The APW program with the muffin-tin potential was used to calculate the $3s$, $3p$, $3d$, and $4s$ energy bands and charge densities. The $3s$ and $3p$ energy bands were calculated at only five high-symmetry points (Γ, H, Δ, N, and P) inside an irreducible wedge that occupied $\frac{1}{48}$th of the Brillouin zone because these energy bands were narrow and far from the Fermi level; the $3s$ band was about 5 Ry below the Fermi level and was about 9 mRy wide for a given spin direction, while the $3p$ band was about 3 Ry deep and about 30 mRy wide for a given spin direction. The spin polarization of both the $3s$ and $3p$ bands was opposite to that of the $3d$ and $4s$ bands; i.e., although the spin-up $3d$ and $4s$ energy bands were below the spin-down $3d$ and $4s$ energy bands, the order was reversed for the $3s$ and $3p$ energy bands. This was also the situation found in ferromagnetic nickel,[15] and was due to the exchange polarization of the $3s$ and $3p$ energy bands by the $3d$ energy bands.[4] The $3d$ and $4s$ energy bands, wider and thus more free-electron-like than the $3s$ and $3p$ energy bands, were calculated using 14 $\vec{k}$ points inside the irreducible wedge.

After calculating new $1s$, $2s$, and $2p$ soft-core charge densities and new $3s$, $3p$, $3d$, and $4s$ APW charge densities, a new iteration was started by calculating a new muffin-tin crystal potential. To avoid oscillations of the iterated energies the new muffin-tin potential was an average of 80% of the potential used in the previous iteration and 20% of the potential calculated from the new charge density. The process of iteration was stopped when the change in the energy bands close to or below the Fermi level was approximately 1 mRy from one iteration to the next. About 20 iterations were required to converge to a self-consistent potential.

From this self-consistent potential the energy bands were calculated at additional points in the irreducible wedge. This was necessary for an accurate calculation of the density of states and determination of the Fermi level as well as for an accurate calculation of the extremal areas of the Fermi surface. To accomplish this, after the final APW iteration using 14 $\vec{k}$ points, the energy bands were found at 55 $\vec{k}$ points in the irreducible wedge, and 9×9 Slater-Koster Hamiltonians[22] were then used to separately fit the spin-up and spin-down energy bands at these 55 $\vec{k}$ points to within 1 mRy. Each of the 9×9 Hamiltonians, using a basis of one s, three p, and five d states and including interactions with third nearest neighbors, contained 44 parameters. This Hamiltonian was then used to generate the energy bands at 285 $\vec{k}$ points inside the irreducible wedge, and the position of the Fermi level was determined by tetrahedral interpolation[23] on the 285 $\vec{k}$ points. We previously noted in niobium[24] that, in order to obtain smooth Fermi-surface contours, an even larger number of $\vec{k}$ points is needed, and therefore we used the Slater-Koster Hamiltonian to generate the energy bands at 1785 $\vec{k}$ points inside the irreducible wedge. The extremal areas of the Fermi surface were then determined from the energy bands on this finer $\vec{k}$-point mesh.

III. DISCUSSION

In Table I we compare calculated magneton numbers with the experimental values. Although our SR values are

TABLE I. Comparison of calculated and experimental magneton numbers (in bohr magnetons).

Lattice constant (a.u.)	Pressure (kbar)	Semirelativistic calculations	Nonrelativistic	Other calculations	Experiment[d]
5.4057 (normal)	0	2.44	2.22	2.16[a], 1.96[b]	2.12
5.2706 (2.5% reduced)	128	2.21	2.21, 2.15[c]	2.15[c]	2.04
5.1354 (5% reduced)	256	2.09	2.23		1.95

[a]Reference 2.
[b]Reference 19.
[c]Reference 4.
[d]Reference 13. The magneton numbers at reduced lattice spacings are calculated from the pressure dependence of the magnetization (Ref. 31).

15% too large, the relative decrease with lattice spacing (-6×10^{-4}/kbar) is in reasonable agreement with experiment. The magneton number at normal pressure from our NR calculation, on the other hand, is closer to the experimental number, but essentially no change with lattice spacing is found.

Callaway and Wang,[2] using the LCGO method, obtained a value for the magneton number of 2.16, which was close to the experimental value, but Greenside and Schlüter,[19] in a recent pseudopotential calculation, found a value of 1.96, which was too small.

The variation in magneton numbers obtained with different approaches points out an important difficulty connected with spin-polarized calculations. That is, the magneton number that results after convergence of a self-consistent calculation may depend upon the initial atomic configurations used as input for calculation of the spin-up and spin-down bands. We found, for example, that after five iterations from a starting configuration corresponding to a magneton number of 0.5, the value remained at approximately 0.5. Although we did not carry out further iterations in order to satisfy our 1-mRy convergence criterion, we believe that the final value for the magneton number would have been close to 0.5. This suggests that there may be more than one value to which a self-consistent, spin-polarized calculation can converge, and it is necessary to calculate total energies in order to establish the magneton number for the ground state. Similar effects have been observed by Janak[18] for fcc cobalt and Greenside and Schlüter[19] for bcc iron.

In Table II the 3*d*-bandwidths are given for both the SR and NR calculation. The widths at the normal lattice spacing are less for the SR bands, and the spin-down widths are greater than the spin-up widths. We also find that the 3*d*-bandwidths increase with pressure, as was the case in nickel.[15] This increase is greater for the SR than the NR calculation. The results of both our calculations are in reasonable agreement with the only experimental value, 228 mRy at symmetry point P.[25]

In Table III we show the variations in the exchange splittings at points Γ, H, and P. At normal lattice spacing the values that we have calculated are larger than those calculated by Callaway and Wang. The splittings of the NR bands change very little with pressure. Eastman *et al.*[25] measured a splitting at point P of 110 mRy, which is about 10% smaller than our NR calculated value.

When the method described in Sec. II was used to calculate the SR Fermi surface at the normal lattice constant, the Fermi surface was found to have a topology that differed qualitatively from the topology determined from dHvA experiments. Because the first-principles SR bands have an H'_{25} spin-up level that is too low, as shown in Fig.

TABLE II. Bandwidths (in mRy).

Lattice constant	$\Gamma_{12}-\Gamma'_{25}$		$H'_{25}-H_{12}$		P_3-P_4	
	Spin up	Spin down	Spin up	Spin down	Spin up	Spin down
a_0 (SR)	102	113	350	424	190	254
a_0 (NR)	108	119	382	453	217	280
a_0 (CW)[a]	102	128	339	383	194	251
Experiment					228[b]	
$0.975a_0$ (SR)	114	124	396	464	215	273
$0.975a_0$ (NR)	113	123	396	465	213	271
$0.95a_0$ (SR)	127	137	451	514	244	297
$0.95a_0$ (NR)	118	128	406	474	206	260

[a]Callaway and Wang (CW), Ref. 2.
[b]Reference 25.

TABLE III. Exchange splittings for first-principles energy bands (in mRy).

Lattice constant	Γ'_{25}	H'_{25}	P_4
a_0 (SR)	185	209	139
a_0 (NR)	168	191	122
a_0 (CW)[a]	134	155	98
Experiment			110[b]
$0.975a_0$ (SR)	171	193	131
$0.975a_0$ (NR)	163	185	122
$0.95a_0$ (SR)	156	176	118
$0.95a_0$ (NR)	165	188	129

[a]Reference 2.
[b]Reference 25.

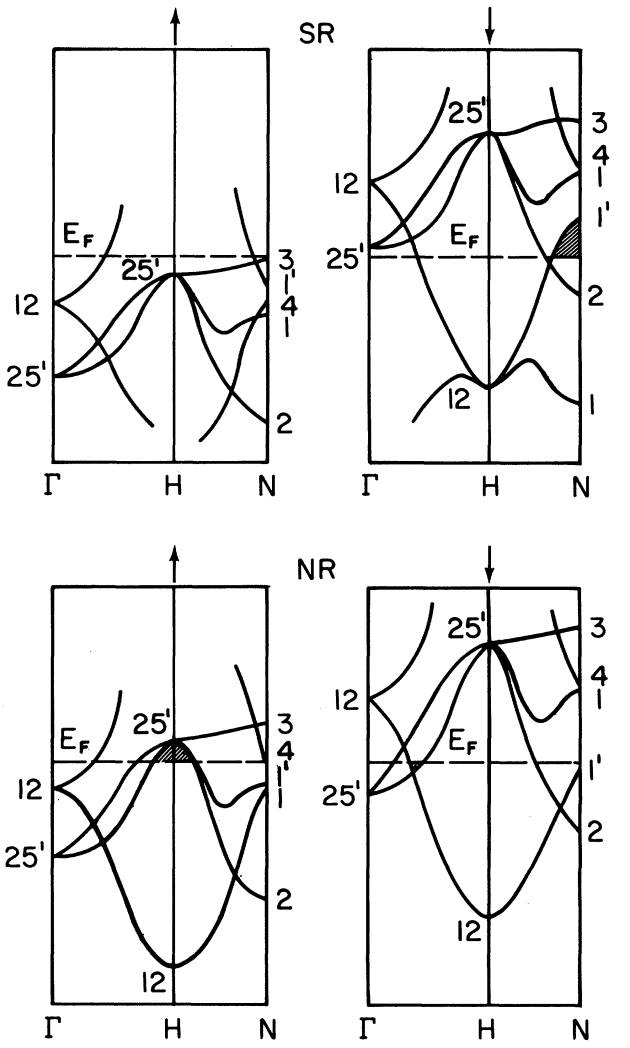

FIG. 1. Schematic representation of energy bands along Γ–H–N. The shaded areas show the hole pockets at point H and the electron balls along line Δ for the NR calculation; these pieces are absent in the SR calculation. The hole pockets at point N are present in the SR calculation, but are missing in the NR calculation.

1, there are no spin-up hole pockets at point H. At the same time the Γ'_{25} spin-down level is too high, which eliminates the electron balls centered along the Γ–H line. Both of these pieces of the Fermi surface have been observed in dHvA experiments.[6–8] Our NR Fermi surface at the normal lattice constant had the right topology, but the agreement with the experimental extremal areas was not as close as in the calculation of Callaway and Wang.[2]

A possible reason for the discrepancies was that the 14-$\vec{k}$-point mesh used to calculate the $3d$ and $4s$ energy bands (Sec. II) did not contain enough points in $\vec{k}$ space. To test this, the SR calculation at the normal lattice constant was repeated, except that the $3d$ and $4s$ energy bands were calculated at 55 $\vec{k}$ points inside the irreducible wedge instead of at 14. After convergence the resulting exchange splitting for the 55-$\vec{k}$-point mesh was only 6 mRy smaller than the exchange splitting for the 14-$\vec{k}$-point mesh at each point in the Brillouin zone. Because an additional, splitting of 56 mRy would be necessary to make the magneton number of the 55-$\vec{k}$-point calculation agree with experiment, we concluded that the size of mesh was not the cause of the discrepancies.

A second possible reason for discrepancies was our use of muffin-tin potential instead of a more general self-consistent potential in which the conditions of spherical symmetry inside the muffin tin and constant potential in the interstitial regions are relaxed. A muffin-tin potential consists of two parts: one part is the spherical potential within the muffin-tin spheres, and the other part is the constant interstitial potential between the spheres. The approximation of a constant interstitial potential is best for close packed structures.[26] For example, the previous APW calculation for spin-polarized nickel by Anderson *et al.*[15] quantitatively reproduced the Fermi surface of nickel, even though it used a muffin-tin potential. Nickel, of course, is a close-packed structure (fcc) and the percentage of the volume of the crystal outside touching muffin-tin spheres is only 26%, while the percentage of the volume of bcc iron outside touching muffin-tin spheres is 32%. Thus, the looser packing of the muffin-tin spheres in bcc iron might be one reason why our first-principles, NR Fermi surface did not agree closely with experiment. Callaway and Wang used a non-muffin-tin potential in their NR LCGO calculation for ferromagnetic iron at the normal lattice constant,[2] and obtained the right topology for the Fermi surface and reasonable agreement with experiment for most of the extremal areas of the Fermi surface.

As far as the spherical potential inside the muffin-tin spheres is concerned, note that in nickel ($3d^8 4s^2$), there are 5.3 electrons per atom in the spin-up bands, and 4.7 electrons per atom in the spin-down bands. Consequently, in nickel both the spin-up and spin-down d bands are almost full, and the charge density has nearly the full symmetry consistent with the cubic structure.[27] Thus the charge density has a distribution close to the spherical symmetry of the free atom, and the muffin-tin approxi-

mation works. In iron ($3d^64s^2$), however, while the spin-up bands contain 5.1 electrons per atom, the spin-down bands have only 2.9 electrons per atom, and thus the $3d$ spin-down bands are about half-full. For the spin-down band, then, the approximation of a spherical charge density inside the muffin-tin spheres is not satisfactory; this is another possible reason why the first-principles NR calculation of the Fermi surface did not agree quantitatively with experiment.

Although the use of the muffin-tin approximation might explain quantitative discrepancies in the NR Fermi surface at the normal lattice constant, it did not explain the incorrect topology of the first-principles Fermi surface for the SR calculation at the normal lattice constant. The effect of the SR terms is shown schematically in Fig. 1. The semirelativistic SR terms raised the spin-down Γ'_{25} and N'_1 energy levels above the Fermi level, although they were below it for the NR calculation. In addition, the SR terms lowered the spin-up H'_{25} energy level below the Fermi level, although it was above it in the NR calculation. The Fermi surface is quite sensitive to relatively small changes that reorder energy levels close to the Fermi level. Such a rearrangement by SR terms was found by Anderson *et al.*[15] in nickel, but this did not have the drastic effect on the Fermi surface of nickel that reordering has on the Fermi surface of iron. In iron the SR terms caused a reordering of the energy levels close to the Fermi level, which significantly changed the first-principles Fermi surface. Another possible cause of the reordering is the use of the von Barth—Hedin exchange, which might not be the correct exchange when relativistic effects are included.[28,29]

To remedy these problems, a constant was added to the spin-up potential of exactly the right magnitude to make the calculated magneton number agree with the experimental magneton number while maintaining the correct number of valence electrons. The spin-down potential was not changed. The constants added to the spin-up potential for the SR calculations were 56 mRy at the normal lattice constant a_0, 37 mRy at $0.975a_0$, and 26 mRy at $0.95a_0$. For the NR calculations, the constants were 24, 32, and 46 mRy, respectively. The added constant uniformly decreased the exchange splitting, although the adjusted splittings varied throughout the Brillouin zone as before. For example, at the normal lattice constant, the SR exchange splitting was decreased by 56 mRy, and the NR exchange splitting was decreased by 24 mRy. These corrections were significantly smaller than the first-principles exchange splittings. When the Fermi surface corresponding to the empirically shifted SR energy bands was calculated (Fig. 2), it was found to have a topology that did qualitatively and quantitatively agree with experiment (Fig. 3). Moreover, when the Fermi surface corresponding to the shifted NR energy bands was calculated, the quantitative agreement with experiment was improved. In Fig. 4 we show the empirically shifted SR energy bands at the normal lattice constant. It is clear now that the electron balls in the spin-down bands and the hole pockets at point H in the spin-up bands exist. Thus, by rigidly shifting the spin-down potential at the normal lattice constant by the amount needed to reproduce the experimental magneton

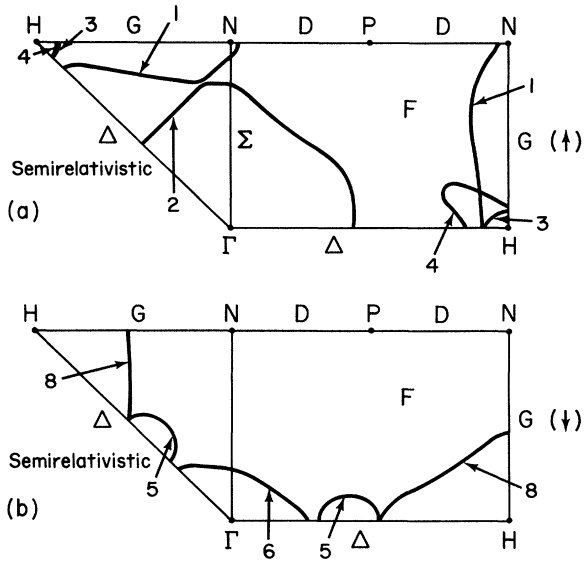

FIG. 2. Cross sections of the Fermi surface in symmetry planes obtained from the SR empirically shifted energy bands. (a) Spin-up Fermi surface: (1) Hole arm along G, (2) electron s-d piece, (3) hole pocket at point H (band 3), and (4) hole pocket at point H (band 4). (b) Spin-down Fermi surface: (5) Electron ball along line Δ; (6) electron octahedron at point Γ, and (8) hole octahedron at point H.

number, the agreement of the calculated and the experimental Fermi surfaces was significantly improved. At the reduced lattice constants, we assumed that the agreement of the calculated and the actual Fermi surfaces would be improved similarly by shifting the spin-down potentials by

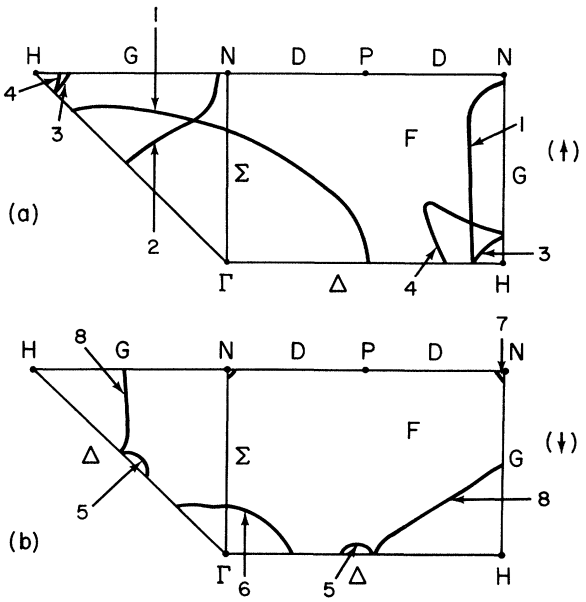

FIG. 3. Experimentally determined cross sections of the Fermi surface in symmetry planes according to Lonzarich (Ref. 8). (a) Spin-up Fermi surface: (1) Hole arm along line G, (2) electron s-d spiece, (3) hole pocket at point H (band 3), and (4) hole pocket at point H (band 4). (b) Spin-down Fermi surface: (5) Electron ball along Δ (6) electron octahedron at Γ, (7) hole pocket at N, and (8) hole octahedron at H.

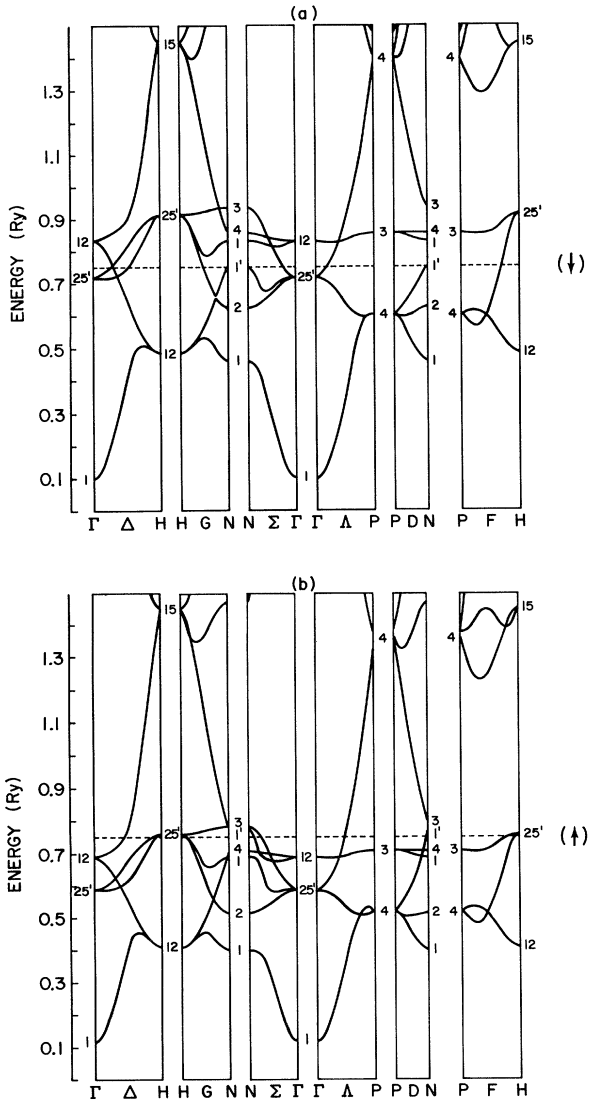

FIG. 4. (a) Empirically shifted spin-down SR energy bands at the normal lattice spacing. (b) Empirically shifted spin-up SR energy bands at the normal lattice spacing.

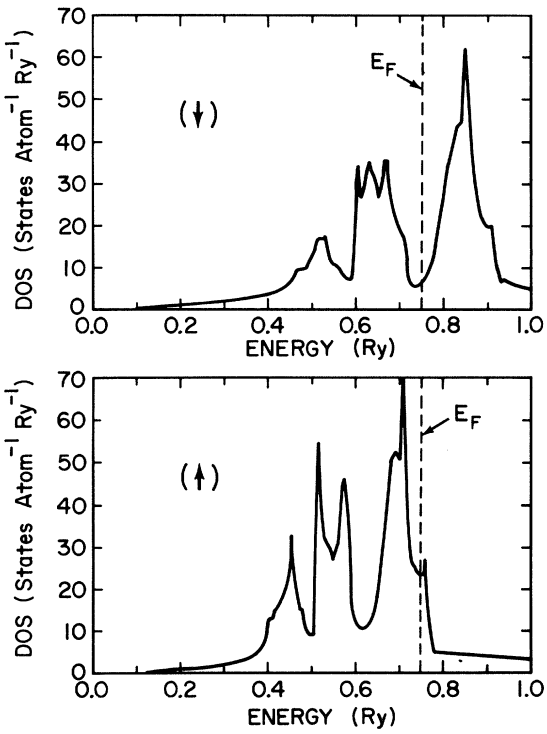

FIG. 5. Densities of states for spin-up and spin-down bands obtained from the SR shifted bands. The Fermi level is denoted by E_F.

the amounts needed to reproduce the experimental magneton numbers. Therefore, we made our calculations of the pressure derivatives of the Fermi surface using the spin-down potentials shifted as described above.

In Fig. 5 the density of states corresponding to the shifted SR bands is shown. We see that the density of states at the Fermi level (E_F) for the spin-up bands is about 4 times the spin-down density of states at E_F. The Fermi level[30] lies at a minimum in the spin-down density of states. The values for the total densities of states at E_F and their angular momentum components for the shifted spin-up and spin-down bands are given in Table IV. From

TABLE IV. Total and decomposed densities of states at E_F for spin-up (↑) and spin-down (↓) shifted bands (in states/atom Ry).

		S	P	t_{2g}	e_g	Total
a_0	SR↑	0.564	0.866	20.2	1.95	23.6
	SR↓	0.004	0.121	5.56	0.872	6.56
	NR↑	0.606	1.05	16.9	2.73	21.3
	NR↓	0.002	0.141	4.99	0.444	5.57
$0.975a_0$	SR↑	0.599	1.04	17.8	2.23	21.6
	SR↓	0.008	0.301	5.70	1.34	7.35
	NR↑	0.609	0.966	17.1	2.74	21.4
	NR↓	0.008	0.393	5.84	1.42	7.66
$0.95a_0$	SR↑	0.623	0.872	14.3	3.01	18.8
	SR↓	0.018	0.194	6.34	2.23	8.78
	NR↑	0.606	0.745	17.4	2.07	20.8
	NR↓	0.049	0.764	7.33	2.91	11.1

TABLE V. Slater-Koster (SK) parameters for shifted energy bands. The entires are in Ry and the notation follows that of Ref. 22 with the abbreviations $d_1 \equiv x^2-y^2$ and $d_2 \equiv 3z^2-r^2$.

SK parameters[a]	a_0 Spin up	a_0 Spin down	$0.975a_0$ Spin up	$0.975a_0$ Spin down
		On site		
$E_{s,s}(000)$	1.1291	1.6731	1.159	1.749
$E_{x,x}(000)$	1.6706	1.562	1.7352	1.650
$E_{xy,xy}(000)$	0.6732	0.7476	0.7238	0.8000
$E_{d_2,d_2}(000)$	0.6318	0.7628	0.6808	0.8150
		First neighbor		
$E_{s,s}(111)$	−0.0883	−0.0986	−0.0910	−0.1025
$E_{s,x}(111)$	−0.0906	−0.0850	−0.0892	−0.0854
$E_{s,xy}(111)$	−0.0532	−0.0340	−0.0556	−0.0334
$E_{x,x}(111)$	0.0923	0.0796	0.0887	0.0749
$E_{x,y}(111)$	0.0699	0.0596	0.0722	0.0634
$E_{x,xy}(111)$	−0.0466	−0.0215	−0.0477	−0.0209
$E_{x,yz}(111)$	−0.0235	−0.0219	−0.0294	−0.0245
$E_{x,d_1}(111)$	0.0241	0.0095	0.0294	0.0118
$E_{xy,xy}(111)$	−0.0108	−0.0122	−0.0122	−0.0135
$E_{xy,xz}(111)$	−0.0167	−0.0194	−0.0188	−0.0214
$E_{xy,d_2}(111)$	−0.0156	−0.0182	−0.0180	−0.0193
$E_{d_2,d_2}(111)$	0.0176	0.0216	0.0198	0.0234
		Second neighbors		
$E_{s,s}(200)$	−0.0480	−0.0492	−0.0477	−0.0457
$E_{s,x}(200)$	−0.0900	−0.1570	−0.0898	−0.1539
$E_{s,d_2}(002)$	−0.0130	−0.0470	−0.0122	−0.0494
$E_{x,x}(200)$	0.1412	0.1915	0.1433	0.1903
$E_{y,y}(200)$	0.0386	−0.0052	0.0365	−0.0078
$E_{x,xy}(020)$	0.0015	0.0289	0.0008	0.0304
$E_{z,d_2}(002)$	−0.0157	−0.0511	−0.0316	−0.0574
$E_{xy,xy}(200)$	0.0038	0.0235	0.0039	0.0249
$E_{xy,xy}(002)$	0.0194	−0.0036	0.0195	−0.0049
$E_{d_2,d_2}(002)$	−0.0266	−0.0336	−0.0308	−0.0365
$E_{d_1,d_1}(002)$	−0.0001	0.0009	0.0003	0.0004
		Third neighbors		
$E_{s,s}(220)$	−0.0017	−0.0408	0.0004	−0.0419
$E_{s,x}(220)$	0.0010	−0.0233	0.0013	−0.0252
$E_{s,xy}(220)$	−0.0013	−0.0067	−0.0006	−0.0076
$E_{s,d_2}(220)$	0.0012	0.0102	0.0008	0.0075
$E_{x,x}(220)$	0.0039	0.0262	0.0041	0.0278
$E_{x,x}(002)$	0.0134	−0.0122	0.0126	−0.0154
$E_{x,y}(220)$	−0.0126	0.0010	−0.0123	0.0110
$E_{x,xy}(220)$	−0.0032	−0.0091	−0.0019	−0.0091
$E_{x,xy}(022)$	−0.0080	0.0010	−0.0075	0.0023
$E_{z,d_2}(022)$	−0.0023	−0.0071	−0.0026	−0.0059
$E_{z,d_1}(022)$	0.0028	0.0062	0.0024	0.0044
$E_{xy,xy}(220)$	−0.0036	−0.0066	−0.0031	−0.0067
$E_{xy,xy}(022)$	−0.0049	0.0011	−0.0049	0.0014
$E_{xy,xz}(022)$	−0.0050	0.0002	−0.0049	0.0007
$E_{yz,d_2}(220)$	0.0000	0.0028	−0.0004	0.0021
$E_{d_2,d_2}(220)$	0.0004	0.0008	0.0007	0.0011
$E_{d_1,d_1}(220)$	−0.0008	−0.0018	−0.0016	−0.0020

[a]These parameters correspond to real matrix elements.

this table we see that the dominant component of the density of states is t_{2g}. It appears to be a general trend that the density of states at E_F for the spin-up bands decreases with pressure, while that for the spin-down bands increases. We may also note that the difference between spin-up and spin-down densities of states at E_F decreases with pressure, as does the magneton number.

Our unshifted SR calculation gave reasonable agreement with the experimentally observed decrease in magneton number with pressure.[31] Because the purpose of the calculation was the determination of trends with pressure, however, consistency demanded shifts of the spin-up potentials at the 2.5% and 5% reduced lattice constants to make the calculated magneton numbers and the experimental magneton numbers agree. The magneton number at the reduced lattice constants was found using the pressure derivative of the magneton number[31] at 4 K (-3.1×10^{-4}/kbar).

The Slater-Koster interpolation method is convenient for representing energy bands. Therefore, in Table V we give the Slater-Koster parameters for the 9×9 matrices that generated shifted energy bands at a_0 (Fig. 4) and at a reduced lattice spacing of $0.975a_0$. We should note that the off-diagonal matrix elements involving s and p orbitals (s,x; s,y; s,z) are imaginary quantities in the Slater-Koster notation.[22] By changing the signs of these matrix elements above the diagonal, and assuming the Slater-Koster Hamiltonian matrix is real, we obtain a real 9×9 matrix with the same eigenvalues as the original matrix. Slater-Koster parameters given in Table V correspond to these real matrices.

IV. SPIN-DOWN FERMI SURFACE

The experimental minority Fermi surface of iron includes four pieces: an electron octahedron centered at point Γ, a hole octahedron centered at point H, a hole pocket centered at point N, and an electron ball along line Δ (Fig. 3). The Fermi surface along Δ is quite sensitive to the crystal potential. The initial dHvA experiments[5,6] were interpreted in terms of a lens and neck along Δ, but more recently, following the calculation of Callaway and Wang, Lonzarich[8] reinterpreted the dHvA data in terms of an electron ball along Δ. Lonzarich also measured low dHvA frequencies which he interpreted as coming from hole pockets in the spin-down bands at N.

A. Electron octahedron at Γ

The experimental areas of the electron octahedron were 10% smaller than the areas for the SR calculation, and they were 19% larger than the areas for the NR calculation (Table VI). The SR calculation also agreed within 5% with the results of the NR LCGO calculation of Callaway and Wang. The experimental effective-mass ratio in the [111] direction is 2.8,[6] which was twice our calculated value. Note that the spin-up and spin-down Γ surfaces were larger pieces with large effective masses. Any piece listed in Table VI that has an effective mass much larger than the effective mass of the Γ surface, i.e., larger than 3, has not been seen experimentally.

In both the NR and SR calculations, the electron octahedron grows isotropically with pressure; i.e., the pressure derivative is the same for the $\langle010\rangle$, $\langle110\rangle$, and $\langle111\rangle$ directions (Table VI).

The Γ electron octahedron had the characteristic shape of a jack (similar to tungsten) at the 2.5% and the 5% reduced lattice constants. At the normal lattice constant no jack was formed since the Δ electron ball did not overlap the Γ octahedron.

B. Hole octahedron at H

The octahedron at H was another piece that had a large area and a large effective mass. The spin-orbit interaction hybridized the spin-down octahedron at H with the spin-up surface at H,[6] and consequently, the experimental dimensions were not expected to agree exactly with an energy-band calculation that neglected the spin-orbit interaction. The calculated areas, however, were within 4% of the experimental areas except for the [110] direction where the calculated area was too large by 25%.

The octahedron at H shrunk under pressure in both the NR and the SR calculations. The rate, however, was an order of magnitude less than the rate at which the electron octahedron grew. The rate of change of area with pressure is smaller along [111] than along [100] or [110].

C. Electron ball

The electron ball along Δ is a small piece of the Fermi surface and is easily observable because its effective mass is small. The areas in the SR and NR calculations are about 4 times and 2 times the experimental areas, respectively. Thus, although the SR calculation came closer to the experimental numbers for the hole octahedron and the electron octahedron, the NR calculation was better for the electron ball. The experimental effective-mass ratio for the [111] extremal area is 0.7,[8] and this agrees with the calculated ratio within 16% (Table V).

Our calculations showed that the electron ball grew under pressure and, like the electron octahedron, the growth was approximately isotropic. This was the only piece for which pressure data existed. The experimental pressure derivative[10] ($\sim0.85\times10^{-2}$/kbar) showed isotropic growth, in agreement with our calculation, but the SR calculation gave a pressure derivative (0.50×10^{-2}/kbar) that was too small, and the NR calculation (1.4×10^{-2}/kbar) was too large by about the same factor. In both calculations the rate of change of area of the electron ball was an order of magnitude greater than the rate of change of the hole octahedron, and it was the same order of magnitude as the rate of change of the electron octahedron.

An interesting effect of pressure was the appearance of the lens-and-neck structure originally proposed as the interpretation of the dHvA data at zero pressure. The lens-and-neck structure appeared when the Δ electron ball grew large enough to overlap the Γ electron jack. The lens was infinitesimal at the 2.5% reduced lattice spacing (128 kbar), but is was quite large at the 5% reduced lattice spacing (256 kbar). The spin-orbit interaction has played an important role in the interpretation of the dHvA data for the electron ball,[8] and indeed, the calculated area re-

TABLE VI. Extremal areas, cyclotron masses, and pressure derivatives for the spin-down and spin-up Fermi surfaces.

Fermi-surface component		Extremal area (MG)[h]			Effective mass ratio (m^*/m)			Pressure derivative ($d\ln A/dP$) (10^{-4}/kbar)		
		[010]	[110]	[111]	[010]	[110]	[111]	[010]	[110]	[111]
		(a) Spin-down Fermi surface								
Γ electron octahedron	SR	79.5	64.5	57.2	2.2	1.8	1.6	27	27	27
	NR	59.4	48.1	42.6	2.0	1.7	1.4	69	69	68
	CW[a]	76	64	59.						
	Expt.[b]	71.0	58.2	52.2 51.8[c]			2.8[c]			
Octahedron at H	SR	233	172	155	2.4	1.6	1.3	−2.5	−1.9	−1.1
	NR	249	181	162	2.5	1.7	1.3	−8.4	−6.5	−5.1
	Expt.	240[d,e]	145[e]	157, 154[c]			1.7[c]			
	CW[a]	248	180	155						
Δ electron ball along [010]	SR	14.6	15.0	15.5	0.79	0.82	0.82	46	48	49
	NR	8.7	9.4	10.0	0.63	0.61	0.60	145	135	132
	CW[a]	5.4								
	Expt.	3.87[d]	4.13[d]	4.15[d,e]			0.71[d]	85[e,f]	90[f]	80[f] 100[d]
Δ electron ball along [001]	SR	15.7	16.8	15.5	0.85	0.86	0.82	45	53	49
	NR	10.5	11.1	10.0	0.62	0.72	0.60	116	137	132
	CW[a]		6.1							
	Expt.	5.05[d]	3.90[d,e]	4.15[d,e]			0.35[c]			
	Expt.	5.04[c]	3.89[c,e]	4.11[c,e]						
		(b) Spin-up Fermi surface								
Electron s-d piece at Γ	SR	386	326	367	2.9	2.1	2.4	3.2	3.4	3.6
	NR	399	335	373	3.5	2.3	2.4	0.1	0.9	2.0
	CW[a]	412	310	373						
	Expt.[b]	436	349, 347[c]	370, 369[c]	2.6[c]					
Hole pockets at H (band 3)	SR	10.3	8.2	7.9	1.1	0.88	0.91	22	25	24
	NR	13.1	10.7	10.1	0.86	0.83	0.52	14	15	12
	CW[a]	7.0	6.9	6.6						
	Expt.	15.0	12.3	11.4						
Hole pockets at H (band 4)	SR	12.5	17.0	14.6	1.3	1.5	1.5	22	21	24
	NR	15.9	21.5	19.0	1.1	1.3	1.5	14	14	15
	CW[a]	9.4	15.5	12.2						
	Expt.	20.6	33.4	27.0						
Arms along G in ($\bar{1}10$) face of Brillouin zone	SR	19.6[g]	3.2[g]	5.0[g]	0.99	0.16	0.34	−12	−62	−59
		17.7	25.1	33.4	0.84	2.0	1.8	−15	20	15
			29.3			1.3			12	
	NR		31.9	100		1.8	2.8		9	12
			33.4			1.3			9	
($\bar{1}01$) face of Brillouin zone	SR		39.1[g]	5.0[g]		2.1	0.34		−7.6	−59
			32.5	33.4		1.4	1.8		−2.1	15
	NR			100			2.8			12
	CW[a]		4.8	8.2						

[a]Reference 2.
[b]Unless otherwise noted, data are from Ref. 7.
[c]Reference 6.
[d]Reference 8.
[e]Hybridized with spin-up Fermi surface.
[f]Reference 10.
[g]These experimental orbits occur in the vicinity of N.
[h]Reference 32.

ported for the electron ball should be larger than the actual areas measured, because the spin-orbit interaction hybridizes the spin-down electron ball with the spin-up *s-d* piece. (Along the [100] direction, however, the magnetic breakdown field is small and the unhybridized, spin-down ball is observed.[8])

Note that a Δ electron ball along the [010] axis gave a different extremal area than a Δ electron ball along the [001] axis for the same orientation of the magnetic field. Table VI therefore distinguishes extremal areas of [010] electron balls from extremal areas of [001] electron balls.

D. Hole pocket at *N*

Lonzarich has interpreted his low-frequency dHvA oscillations (Table VII) as belonging to a small hole pocket at *N*. Callaway and Wang[2] found a hole pocket at *N* in their calculation at the normal lattice constant, but it was larger than experiment by a factor of 11. Our SR calculation showed such a hole pocket, but it was infinitesimally small at the normal lattice constant because the N_1' energy level (Fig. 4) was only 1 meV above the Fermi level. The pocket was absent in our NR model at the normal lattice constant. This shows how sensitive the levels at *N* are to the various assumptions made in a band calculation.

V. SPIN-UP FERMI SURFACE

The experimental majority Fermi surface includes four pieces (Fig. 3): an electron *s-d* piece at Γ, two hole pockets at *H*, and hole arms along the line from *H* to *N*, i.e., along *G*. The Γ *s-d* piece is the largest of all the observable pieces of both the spin-up and spin-down surfaces. This piece, together with the two spin-up hole pockets at *H* and the spin-down Γ electron octahedron, comprise the four pieces of the Fermi surface that unequivocally exist and whose dimensions are accurately known. Whether the arms along *G* are connected or pinched off depends on the lattice constant; this topology has important implications for the interpretation of the magnetoresistance data.[9]

A. Electron *s-d* piece

Both the SR and NR calculations at the normal lattice constant reproduced the areas of the large *s-d* piece at Γ rather well. For the [111] direction, both calculations were within 1% of the experimental value (Table VI). Since the effective masses were greater than 2, the amplitude of dHvA oscillations should be small.

The *s-d* piece at Γ grew under pressure, but like the spin-down hole octahedron, the change was slight ($\sim 10^{-4}$/kbar). Moreover, when going from the 2.5% reduced lattice constant to the 5% reduced lattice constant, the SR calculation showed that the Γ surface increased slightly, while the NR calculation showed a decrease. From these results we predict that the pressure derivative of the area of the spin-up electron *s-d* piece is at least a factor of 2 smaller than the pressure derivatives of the other spin-up pieces.

B. Hole pockets at *H*

At the normal lattice constant, the SR and NR calculated areas of the band-3 hole pocket at *H* were about 30% and 13% smaller, respectively, than the experimental areas (Table VI). The agreement for the band-4 hole pocket was worse. The SR calculation gave areas about 50% too small, while the NR calculated areas were about 30% too small. Thus the NR calculation was better than the SR calculation for both sets of pockets at *H*. Furthermore, we may note that both the SR and NR calculations were closer to experiment than the calculation of Callaway and Wang[2] for these pockets. The effective masses for the spin-up hole pockets at *H* were 2 to 3 times smaller than the effective masses of the spin-up *s-d* piece.

Our calculations showed that at low pressures both sets

TABLE VII. Extremal areas and cyclotron masses, for the spin-down hole pockets at *N* at 128 kbar.

Orientation		Extremal area (MG)[c] [010]	[110]	[111]	Effective-mass ratio (m^*/m) [010]	[110]	[111]
Hole pockets at *N* (110) face	SR	4.03	3.34	3.23	0.36	0.31	0.31
	NR	5.53	4.64	4.52	0.36	0.31	0.28
	CW[a]	16	15.8	15.4			
	Expt.[b]	1.44	1.37	1.35			
($\bar{1}$01) face	SR	3.24	3.54	4.13	0.26	0.29	0.31
	NR	4.36	4.73	5.53	0.27	0.28	0.34
	CW[a]	16		19.2			
	Expt.	1.30	1.51	1.45			
($\bar{1}$10) face	SR	4.03	4.96	4.13	0.36	0.43	0.31
	NR	5.53	6.90	5.53	0.36	0.43	0.34
	CW[a]	16	19.6	19.2			
	Expt.[b]	1.44	1.37	1.45			

[a]Reference 2.
[b]Reference 8 (experimental values at the normal lattice spacing).
[c]Reference 32.

of hole pockets at H grew with increasing pressure for the SR (2.5×10^{-3}/kbar) and the NR (1.5×10^{-3}/kbar) calculations, and the rate of growth is nearly an order of magnitude larger than for the spin-up *s-d* piece. When going from the 2.5% reduced lattice constant to the 5% reduced lattice constant, the hole pockets continued to grow for the SR calculation, but not linearly with pressure, while for the NR calculation, they actually shrank. The growth from the normal lattice constant to the 2.5% reduced lattice constant was nearly isotropic for both the SR and the NR calculations.

C. Hole arms along G

The spin-up hole arms along G had the most complicated sets of orbit of all the pieces of the Fermi surface of iron (Table VI). At the normal lattice constant, the hole arms in the SR calculation were connected at N and they ran continuously from H to N and across to the next H point. First of all, this meant that there were open orbits in the $\langle 110\rangle$ directions, which was consistent with magnetoresistance data.[9] Secondly, the connection at N meant there were more extremal cross-sectional areas than if the arms were not connected at N, because the N point has inversion symmetry, and thus any plane that passed through N and intersected the connected arms was an extremal plane. The arms in the NR calculation at the normal lattice constant, however, were not connected at N. The experimental situation was much simpler. Only a few dHvA frequencies were observed and this was attributed to the fact that extremal sections of the hole arms are expected to have large cyclotron masses.

The SR and NR calculations were in disagreement over the behavior of the arms under pressure. According to the SR calculation, the hole arms were connected at N, but as the pressure increased they were pinched off. The behavior was just the opposite according to the NR calculation, where the hole arms were pinched off at N for the normal lattice constant, but as the pressure increased they become connected. We should note, however, that in the SR calculation, the change of the arms from connected at N to pinched off at N did not take place until the pressure was above 130 kbar, at which point there was a phase transition from the bcc structure to the hcp structure. In the NR calculation, however, the change from arms pinched off at N to arms connected at N took place below the pressure of the phase transition. The pressure derivatives of the hole arms were the same order of magnitude as the pressure derivatives of the hole pockets at H, but in some cases had negative signs. The extra frequencies introduced when the arms are no longer pinched off at N, as predicted by the NR calculation, should have mass ratios less than 0.5.

Note that arms in different faces of the Brillouin zone give different extremal areas for a given orientation of the magnetic field. Table VI gives tabulated extremal areas for different faces in which an arm can lie. The situation is even more complicated, however, because an arm on a given face of the Brillouin zone has several extremal areas, and thus Table VI tabulates several extremal areas for each face and each field orientation. Table VI has been simplified by omitting extremal areas with effective masses larger than 4, since these are unlikely to be experimentally observable.

VI. CONCLUSIONS

Fermi-surface—area comparisons have not permitted us to choose between the SR and the NR calculations. The NR spin-up Fermi surface was in slightly closer agreement with the experimental Fermi surface, but the SR spin-down Fermi surface was closer to the experimental Fermi surface than the NR spin-down Fermi surface; an exception was the spin-down Δ electron ball, where the NR spin-down Fermi surface was closer.

Because of the extremely limited amount of data on the influence of pressure on the Fermi surface (only the spin-down electron ball has been investigated), pressure derivatives do not provide any criterion for choosing between our SR and NR calculations. Therefore we have presented results from both models. For most pieces of the Fermi surface the SR pressure derivatives and the NR pressure derivatives agreed only with respect to sign and order of magnitude. Thus, only the sign and the order of magnitude of the calculated pressure derivatives in Table VI are reliable. For example, although the calculated pressure derivatives for the spin-down Δ electron ball had the right order of magnitude, the SR calculation was about a factor of 2 too small and the NR calculation was a factor of 2 too large.

We can, however, make the following predictions about the behavior of the Fermi surface of iron under pressure. The spin-up *s-d* piece grows slightly under pressure and the rate of growth is roughly 10^{-4}/kbar. The spin-down octahedron at H shrinks slightly under pressure and the rate is roughly the same as for the *s-d* piece, viz., 10^{-4}/kbar. The octahedron at H shrinks fastest in the $\langle 010\rangle$ directions. Both the band-3 and the band-4 spin-up hole pockets at H grow isotropically under pressure at identical rates, i.e., roughly 10^{-3}/kbar. The spin-down Γ electron octahedron also grows with pressure at a rate of roughly 10^{-3}/kbar. The spin-down Δ electron ball grows under pressure faster than any other piece of the Fermi surface. The rate of growth is roughly 10^{-2}/kbar and is isotropic.

ACKNOWLEDGMENTS

We wish to thank the University of Maryland for use of computing facilities, and the U.S. Naval Research Laboratory for providing computer time. We are indebted to L. L. Boyer, C. S. Wang, and S. H. Vosko for helpful discussions and suggestions.

*Present address: Laboratory for Physical Sciences, 4928 College Avenue, College Park, MD 20740.

[1]J. H. Wood, Phys. Rev. 126, 517 (1962).

[2]J. Callaway and C. S. Wang, Phys. Rev. B 16, 2095 (1977).

[3]U. von Barth and L. Hedin, J. Phys. C 5, 1629 (1972).

[4]V. L. Moruzzi, J. F. Janak, and A. R. Williams, *Calculated Electronic Properties of Metals* (Pergamon, New York, 1978).

[5]L. I. Vinokurova, A. G. Gapotchenko, E. S. Itskevich, E. T.

Kulatov, and N. I. Kulikov, Zh. Eksp. Teor. Fiz. 76, 1644 (1979) [Sov. Phys.—JETP 49, 834 (1979)].
[6]A. V. Gold, L. Hodges, P. T. Panousis, and D. R. Stone, Int. J. Magn. 2, 357 (1971).
[7]D. R. Baraff, Phys. Rev. B 8, 3439 (1973).
[8]G. G. Lonzarich, in *Electrons at the Fermi Surface,* edited by M. Springford (Cambridge University Press, Cambridge, 1980), Chap. 6.
[9]R. V. Coleman, W. H. Lourey, and J. A. Polo, Jr., Phys. Rev. B 23, 2491 (1981).
[10]L. I. Vinokurova, A. G. Gapotchenko, and E. S. Itskevich, Zh. Eksp. Teor. Fiz. Pis'ma Red 28, 280 (1978) [JETP Lett. 28, 256 (1978).
[11]T. Takohashi and W. A. Basset, in *Advances in High Pressure Research,* edited by R. S. Bradley (Academic, New York, 1974), Vol. 4, p. 208.
[12]G. C. Kennedy and S. N. Vaidya, J. Phys. Chem. Solids 31, 2329 (1970).
[13]H. Danan, A. Herr, and A. J. P. Meyer, J. Appl. Phys. 39, 669 (1968).
[14]D. A. Papaconstantopoulos, in *Metal Hydrides,* edited by Bambakidis, Nato Advanced Study Institute Series (Plenum, New York, 1981), Ser. B, Vol. 76, pp. 215–242.
[15]J. R. Anderson, D. A. Papaconstantopoulos, L. L. Boyer, and J. E. Schirber, Phys. Rev. B 20, 3172 (1979).
[16]D. D. Koelling and B. N. Harmon, J. Phys. C 10, 3107 (1977).
[17]A. V. Gold, J. Low Temp. Phys. 16, 3 (1974).
[18]J. F. Janak, Solid State Commun. 25, 53 (1978).
[19]H. S. Greenside and M. A. Schlüter, Phys. Rev. B 27, 3111 (1983).
[20]F. Herman and S. Skillman, *Atomic Structure Calculations* (Prentice-Hall, Englewood Cliffs, N. J., 1963).
[21]D. A. Liberman, D. T. Cromer, and J. T. Waber, Comput. Phys. Commun. 2, 107 (1971).
[22]J. C. Slater and G. F. Koster, Phys. Rev. 94, 1498 (1954).
[23]G. Lehmann and M. Taut, Phys. Status Solidi B 54, 469 (1972).
[24]J. R. Anderson, D. A. Papaconstantopoulos, and J. E. Schirber, Phys. Rev. B 24, 6790 (1981).
[25]D. E. Eastman, F. J. Himpsel, and J. A. Knapp, Phys. Rev. Lett. 44, 95 (1980).
[26]L. F. Mattheiss, J. H. Wood, and A. C. Switendick, in *Methods in Computational Physics,* edited by B. Alder, S. Fernbach, and M. Rotenberg (Academic, New York, 1968), Vol. 8, p. 63.
[27]L. M. Falicov, *Group Theory and Its Physical Applications* (University of Chicago Press, Chicago, 1966), p. 118.
[28]A. H. MacDonald, J. M. Daans, S. H. Vosko, and D. D. Koelling, Phys. Rev. B 25, 713 (1982).
[29]A. H. MacDonald, J. Phys. C 16, 3869 (1983).
[30]The Fermi level for the SR calculation is 751.0 mRy at the normal lattice spacing and 811.5 mRy at the 2.5% reduced lattice spacing.
[31]E. I. Kondorskii and V. L. Sedov, Zh. Eksp. Teor. Fiz. 38, 773 (1960) [Sov. Phys.—JETP 11, 561 (1960)].
[32]The extremal areas in $\vec{k}$ space have been expressed in units of magnetic field(MG): area(MG)$=1.047\,28\times$area(nm^{-2}).